







Quantum size effects in the magnetic susceptibility of a metallic nanoparticleM. Roda-Llordes ^{1,2,*} C. Gonzalez-Ballester ^{1,2} A. E. Rubio López ^{1,2} M. J. Martínez-Pérez ^{3,4}
F. Luis ³ and O. Romero-Isart ^{1,2,†}¹*Institute for Quantum Optics and Quantum Information of the Austrian Academy of Sciences, A-6020 Innsbruck, Austria*²*Institute for Theoretical Physics, University of Innsbruck, A-6020 Innsbruck, Austria*³*Instituto de Ciencia de Materiales de Aragón, CSIC-Universidad de Zaragoza, E-50009 Zaragoza, Spain*⁴*Fundación ARAID, Avda. de Ranillas, E-50018 Zaragoza, Spain*

(Received 3 November 2020; revised 17 August 2021; accepted 23 August 2021; published 10 September 2021)

We theoretically study quantum size effects in the magnetic response of a spherical metallic nanoparticle (e.g., gold). Using the jellium model in spherical coordinates, we compute the induced magnetic moment and the magnetic susceptibility for a nanoparticle in the presence of a static external magnetic field. Below a critical magnetic field the magnetic response is diamagnetic, whereas above such field the magnetization is characterized by sharp, steplike increases of several tenths of Bohr magnetons, associated with the Zeeman crossing of energy levels above and below the Fermi sea. We quantify the robustness of these regimes against thermal excitations and finite linewidth of the electronic levels. Finally, we propose two methods for experimental detection of the quantum size effects based on the coupling to superconducting quantum interference devices.

DOI: [10.1103/PhysRevB.104.L100407](https://doi.org/10.1103/PhysRevB.104.L100407)

Metal clusters lie in between the realms of bulk metals and atoms [1,2]. Determining the size at which the metallic behavior arises is not easy as it depends on which physical quantity one uses to define “metallicity.” Some properties, such as the crystal structure or average bonding distances, converge to bulk values surprisingly quickly and, in the case of, e.g., the electron density, even for clusters of less than 200 atoms [3]. By contrast, clear deviations from bulk values are found in other properties for much larger nanoparticles. Two notable examples are the large charging energy of nanoscopic metal clusters [4] and the size-dependent optical absorption in plasmonic nanoparticles [5]. Many of these phenomena stem from the nanoscale spatial confinement of the electronic wave functions. The resulting, atomlike discrete energy level structure gives way, as the particle size increases, to a bulklike quasicontinuum band structure. In the intermediate regime, the response of metallic structures can still show evidence of finite energy gaps or correlations between different levels. Such *quantum size effects* have a strong impact in, among others, the electric conductance through metallic nanobridges [6], or the temperature and magnetic field dependence of the specific heat in, e.g., Pd clusters [7].

In this Letter we study quantum size effects in the magnetic response of a spherical metallic nanoparticle and discuss their experimental observation. Motivated by previous theoretical approaches based on the simplest picture of spinless free electrons [8–10], which have been applied to explore the orbital magnetism [9,11] of metallic clusters, we describe the nanoparticle using the jellium model. This model is simple enough to allow for a numerically exact solution, while

complex enough to successfully describe quantum size effects such as, e.g., the minima in ionization potential of Na and K clusters with full electronic shells [12,13]. The jellium model is a particularly good description for high-density materials with free-electron-like conduction bands dominated by *s* orbital electrons, especially alkali metals [14]. Since the high reactivity of these metals makes nanoclusters only available in jets [13], we focus on Au nanoparticles whose equilibrium magnetic response is easier to observe experimentally. Gold combines a simple electronic structure, dominated by the outer $6s^1$ orbitals [15] with excellent chemical stability. The jellium model provides a good description for gold whereby relativistic effects (e.g., spin-orbit coupling) can be safely neglected [16,17]. Furthermore, Au nanoparticles with well controlled and homogeneous sizes and shapes can be chemically synthesized, stored in the form of colloids for long periods of time [5,18,19], and individually transferred to an on-chip location (e.g., above a magnetic sensing device to measure their magnetic response) with the tip of an atomic force microscope [20].

We consider a rigid, spatially fixed metallic nanosphere of radius R in the presence of a homogeneous magnetic field $\mathbf{B}(\mathbf{r}) = B_0 \mathbf{e}_z$. We describe its internal electronic degrees of freedom using the jellium model [14,21,22], i.e., we describe the particle as an ensemble of N free electrons under the influence of a positively charged background, whose effect is to create an infinite spherical potential well of radius R for the electrons. The only material-dependent free parameter within this model is the electronic density $N/V \equiv 3N/(4\pi R^3)$, usually given through the Wigner-Seitz radius $r_s \equiv R/N^{1/3}$ [14]. The Hamiltonian of the nanoparticle within this model is given by $\hat{H} = \hat{H}_0 + \hat{H}_B$. The first term describes the dynamics of its electrons for $B_0 = 0$, namely, $\hat{H}_0 = \sum_{i=1}^N \hat{\mathbf{p}}_i^2/(2m_e) + U\Theta(|\hat{\mathbf{r}}_i| - R)$ with $U \rightarrow \infty$. Here $\Theta(x)$ is the Heaviside

*marc.roda-llordes@uibk.ac.at

†oriol.romero-isart@uibk.ac.at

step function, m_e the electron mass, and $\hat{\mathbf{r}}_i = (\hat{x}_i, \hat{y}_i, \hat{z}_i)$ and $\hat{\mathbf{p}}_i$ the position and momentum operator vectors of the i th electron. As \hat{H}_0 is spherically symmetric we choose a single-particle eigenstate basis $\{|nlms\rangle\}$ composed by eigenstates of the orbital and spin angular momentum operators, i.e., $[\hat{L}^2, \hat{L}_z, \hat{S}_z]|nlms\rangle = \hbar[\hbar l(l+1), m, s]|nlms\rangle$ with $n \in \mathbb{N}$, $l \in \mathbb{N}_0$, $m \in \mathbb{Z}$ with $|m| \leq l$, and $s = \pm 1/2$, respectively. Importantly, the corresponding eigenenergies, given by $E_{nl} = E_0 u_{ln}^2$ with $E_0 \equiv \hbar^2/(2m_e R^2)$ and u_{ln} the n th zero of the spherical Bessel function of the first kind of order l (see Supplemental Material [23] for details), are highly discretized due to the electronic confinement within the nanoparticle [1,4,21,24]. The term of the Hamiltonian describing the effect of the homogeneous magnetic field reads [16,23]

$$\hat{H}_B = \hbar\omega_L \frac{\hat{L}_z + 2\hat{S}_z}{\hbar} + \frac{1}{2}m_e\omega_L^2\hat{\rho}^2, \quad (1)$$

where $\omega_L \equiv eB_0/(2m_e)$, $e > 0$ is the fundamental charge, $\hat{L}_z \equiv \sum_i \hat{L}_{z,i}$, $\hat{S}_z \equiv \sum_i \hat{S}_{z,i}$, and $\hat{\rho}^2 \equiv \sum_i (\hat{x}_i^2 + \hat{y}_i^2)$. We are interested in the regime of nanometer-size particles and moderate B fields ($\eta \equiv eB_0 R^2/\hbar \ll 1$), which allows us to treat the second term of Eq. (1) perturbatively [23]. We consider as unperturbed eigenstates the single-particle eigenstates of \hat{H}_0 , namely, $|nlms\rangle$, which are also eigenstates of the first term in Eq. (1). The eigenenergies up to first order in perturbation theory are hence given by

$$\frac{E_{nlms}}{E_0} = u_{ln}^2 + \eta(m + 2s) + \frac{\eta^2}{4R^2} \langle nlms | \hat{\rho}^2 | nlms \rangle. \quad (2)$$

The effect of the homogeneous magnetic field is thus to lift degeneracies in analogy with the Zeeman effect and to add a small diamagnetic energy to all eigenstates.

We are interested in the induced magnetic dipole of the sphere, given by the operator [25]

$$\hat{\mathbf{m}} = -\frac{\mu_B}{\hbar} \sum_{i=1}^N (\hat{\mathbf{r}}_i \times [\hat{\mathbf{p}}_i + e\mathbf{A}(\hat{\mathbf{r}}_i)] + 2\hat{\mathbf{S}}_i), \quad (3)$$

where $\mu_B \equiv \hbar e/(2m_e)$ is the Bohr magneton and $\mathbf{A}(\mathbf{r})$ the electromagnetic vector potential. Owing to the symmetry of the system, the expected value of Eq. (3) for a thermal state of \hat{H} at temperature T is parallel to the homogeneous magnetic field, i.e., $\langle \hat{\mathbf{m}} \rangle = m_z \mathbf{e}_z$ with

$$m_z = -\mu_B \left(\frac{\langle \hat{L}_z \rangle}{\hbar} + 2 \frac{\langle \hat{S}_z \rangle}{\hbar} + \frac{eB_0}{2\hbar} \langle \hat{\rho}^2 \rangle \right). \quad (4)$$

The first two terms contribute to the paramagnetic response of the system, as states with negative orbital and spin angular momenta are energetically favored [see Eq. (2)]. Conversely, the third term in Eq. (4) corresponds to a diamagnetic contribution.

Evaluating Eq. (4) requires calculating expected values of single-particle operators of the form [14]

$$\langle \hat{O} \rangle = \sum_{nlms} \bar{n}_{nlms}(T) \langle nlms | \mathcal{O}(\hat{\mathbf{r}}, \hat{\mathbf{p}}, \hat{\mathbf{S}}) | nlms \rangle. \quad (5)$$

Here $\bar{n}_{nlms}(T) \equiv f_{\text{FD}}(E_{nlms}, \mu, T)$ is the mean thermal occupation of the electronic level $|nlms\rangle$, with $f_{\text{FD}}(E, \mu, T) = (1 + \exp[(E - \mu)/(k_B T)])^{-1}$ the Fermi-Dirac distribution and k_B the Boltzmann constant. The chemical potential μ is defined implicitly via

$$N = \left(\frac{R}{r_s} \right)^3 = \sum_{nlms} \bar{n}_{nlms}(T). \quad (6)$$

At $T = 0$ it defines the Fermi energy $E_F \equiv \mu(T = 0)$, whereby $\bar{n}_{nlms}(T = 0) = \Theta(E_F - E_{nlms})$. To accurately model the physical conditions in the experimental proposal below, the number of electrons N is assumed fixed. Thus, to compute observables from Eq. (5), one first needs to solve Eq. (6) to obtain the (N, T, B_0) -dependent chemical potential $\mu(T, N, B_0)$. Even in the simplest case $T = B_0 = 0$, this is an involved task as it requires one to determine, for a given value of N (i.e., for a given radius R), the lowest N single-particle eigenenergies E_{nlms} . This is difficult in practice for two reasons. First, the small size of the particle discards a continuum limit approach. Second, the spherical boundary conditions result in eigenenergies E_{nlms} which, as opposed to other cases (e.g., cubic box boundary conditions [8–10]) do not obey an absolute ordering rule, as the zeros of the spherical Bessel functions are interlaced in a complex way. In other words, no absolute rule exists to determine which of two arbitrary zeros, u_{ln} and $u_{l'n'}$, is the largest. As shown in detail in [23], we have developed a numerical algorithm that allows us to solve Eq. (6) exactly at $T = 0$, and numerically with arbitrary precision at $T \neq 0$, for the range of nanoparticle sizes we are interested in ($R \lesssim 40$ nm).

The induced dipole moment m_z , Eq. (4), is shown in Fig. 1(a) as a function of external field B_0 for a gold nanoparticle ($r_s = 3a_0$ with a_0 the Bohr radius) with radius $R = 7.5$ nm at three different temperatures. The induced moment shows two distinct behaviors delimited by a critical field $B_0 = B_*$, to be defined and analyzed below. At fields $B_0 < B_*$ the response is diamagnetic, $m_z \propto -B_0$, whereas at large enough fields $B_0 > B_*$ the magnetic moment not only starts to increase with B_0 , but does so in quantized jumps of several tens of Bohr magnetons, equivalent in magnitude to sudden flips of several tenths of electronic spins at once. This quantized behavior is more pronounced at zero temperature [red line in Fig. 1(a)], and gradually smears away upon increasing T . Note that the transition from decreasing to increasing behavior in m_z , at $B_0 = B_*$, remains for higher temperatures.

The magnetic response of the nanosphere shown by Fig. 1(a) can be understood from the single-particle eigenenergies in Eq. (2). At $T = B_0 = 0$, the electronic ground state corresponds to the states with the lowest N eigenenergies being occupied, and fulfills $\langle \hat{L}_z \rangle = \langle \hat{S}_z \rangle = 0$ [26]. When a magnetic field B_0 is applied, the zero-field eigenenergies become nondegenerate, as states with different values of m and s experience a Zeeman splitting [see Eq. (2)]. At weak fields $B_0 < B_*$ these energy shifts are small, and states above and below the original Fermi level remain well separated. The ground state is thus the same as at zero field, resulting in a diamagnetic response $m_z = -B_0 \mu_B e \langle \hat{\rho}^2 \rangle / (2\hbar)$ [see Eq. (4)]. Conversely, at strong enough fields $B_0 > B_*$, the Zeeman-split

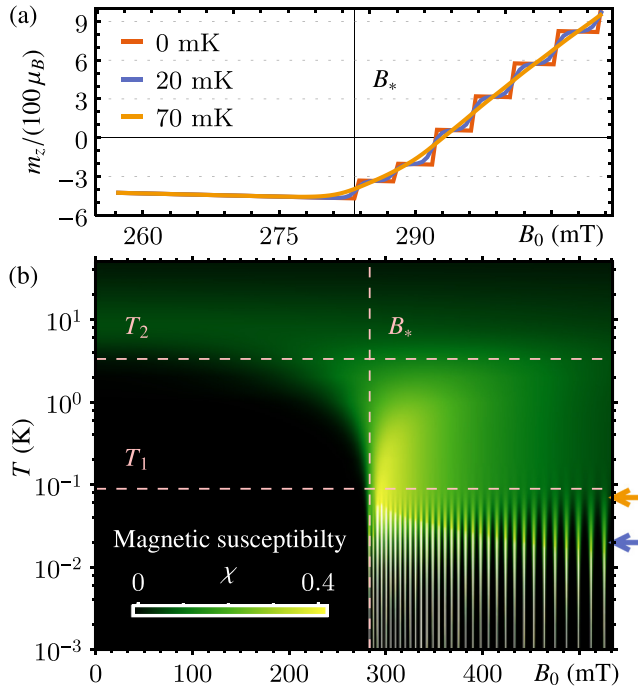


FIG. 1. (a) Induced magnetic dipole moment m_z [Eq. (4)] in a nanoparticle with radius $R = 7.5$ nm as a function of applied magnetic field B_0 , and at temperatures $T = 0$ (red), 20 mK (blue), and 70 mK (yellow). (b) Magnetic susceptibility χ [Eq. (7)] as a function of B_0 and T for the same nanoparticle as above. The dashed lines indicate the critical field B_* and temperatures T_1 and T_2 (see main text for details). The colored arrows indicate the values of T shown in panel (a). All panels correspond to gold ($r_s = 3a_0$).

states originally above and below the Fermi level start to overlap, and the ground state changes abruptly when a previously occupied state $|n_1, l_1, m_1, s_1\rangle$ becomes empty while a previously empty state $|n_2, l_2, m_2, s_2\rangle$ becomes occupied. As a result, the induced magnetic dipole moment sharply changes by an amount $\mu_B[(m_2 + 2s_2) - (m_1 + 2s_1)]$, typically of many Bohr magnetons due to the high values of the orbital quantum numbers l and m near the Fermi level. Since $|s| \leq 1/2$, the effects of the spin degree of freedom are negligible in comparison, as expected [27]. At higher temperatures, the field-induced modification of the ground state is still present but the sharp changes in m_z become less appreciable as the mean occupation number of states above and below the Fermi level is no longer 0 or 1 but given by the smoother function $\bar{n}_{nlms}(T)$. We remark that both the sudden slope change at $B_0 = B_*$ and the steplike behavior of m_z are quantum size effects as they stem from the discrete character of the single-electron energy levels $E_{nl} \propto R^{-2}$ and the Pauli exclusion principle.

In order to further characterize the magnetic response of the nanosphere, we compute the point-particle magnetic susceptibility [16], which we define as

$$\chi \equiv \frac{\mu_0}{V} \frac{\partial m_z}{\partial B_0}, \quad (7)$$

with μ_0 the vacuum permeability. We display χ in Fig. 1(b) as a function of temperature T and applied field B_0 . The mag-

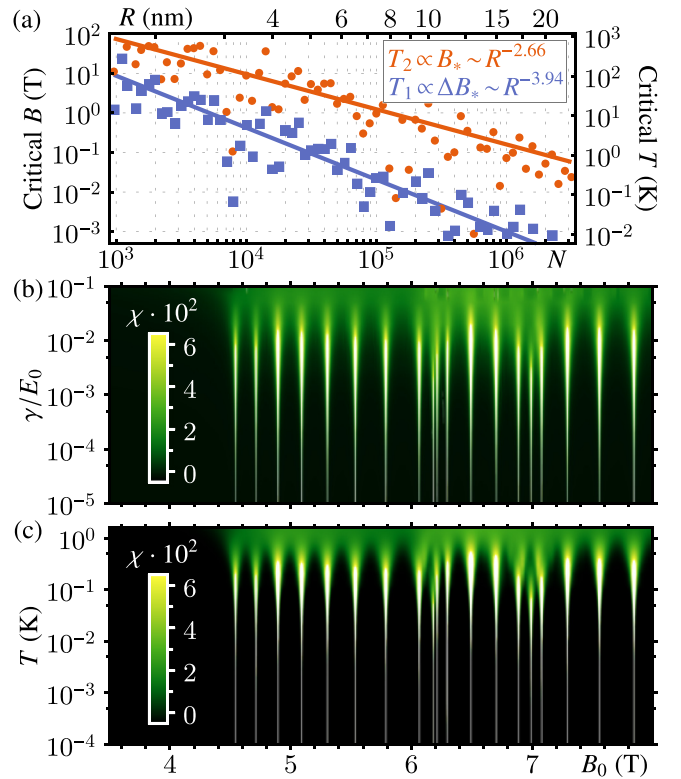


FIG. 2. (a) Critical fields and temperatures (B_* , T_2) (red) and (ΔB_* , T_1) (blue) as a function of electron number N (lower axis) or particle radius R (upper axis). Solid lines show the fit to a power law. (b) Zero-temperature magnetic susceptibility [Eq. (7)] of a nanoparticle with $R = 3.7$ nm as a function of applied field B_0 and linewidth of the single-electron levels γ . (c) Magnetic susceptibility as a function of temperature T for $\gamma = 0$ and the same nanoparticle as in (b). All panels correspond to gold ($r_s = 3a_0$).

netic response shows different regimes as a function of T and B_0 , delimited by three critical parameters, namely, B_* , T_1 , and T_2 . The critical field B_* , already introduced above, can now be rigorously defined as the field at which the first energy level crossing occurs at $T = 0$. This corresponds to the first sharp peak in the susceptibility χ in the low-temperature regime $T \rightarrow 0$. Furthermore, we define two critical temperatures as $T_1 \equiv 35\mu_B(\Delta B_*)/(2k_B)$ and $T_2 \equiv 35\mu_B B_*/(2k_B)$, where ΔB_* is the separation between B_* and the magnetic field at which the *second* level crossing occurs at $T = 0$, namely, the second susceptibility peak at $T \rightarrow 0$. As shown by Fig. 1(b), the critical temperature T_1 corresponds to the temperature above which the steplike behavior of the magnetic response disappears due to thermal effects. Finally, at temperatures above T_2 , the Fermi-Dirac distribution reaches out far above the Fermi level and the discretization of the electronic levels becomes irrelevant, resulting in a magnetic response monotonically dependent on B_0 .

The various susceptibility regimes described above remain for a wide range of particle sizes R , as demonstrated in [23] where we provide identical figures as Fig. 1(b) for $R = 4, 5, 9, \text{ and } 14$ nm. However, the critical parameters B_* , T_1 , and T_2 decrease with increasing particle size, as shown by Fig. 2(a), where we display B_* and ΔB_* calculated exactly as a function of particle size ($*$ axis) and the corresponding

T_1 and T_2 (right axis). The dependence on the radius R is not smooth since the Fermi level changes abruptly with the radius, but is well fitted by a power dependence $R^{-\alpha}$, with $\alpha = 2.66 \pm 0.62$ and $\alpha = 3.94 \pm 0.99$ for B_* and ΔB_* , respectively. These values of α reflect a quantum size effect as they can be related to the size dependence of the energy spacing between electronic levels, $E_0 \propto R^{-2}$, and the fact that the maximum available values for the quantum numbers l, m increase with increasing particle size. The decrease of the critical parameters with the particle size hinders, for too large particles, the experimental observation of the exotic magnetic response shown by Fig. 1(a).

The magnetic response predicted by our ideal model of isolated, noninteracting electrons is expected to remain in realistic experimental conditions. Deviations from our model could stem from electron-electron or electron-phonon interactions, surface roughness, or interactions with the particle substrate, among others. We describe the effect of all these deviations through the addition of a phenomenological linewidth γ to each electronic level [14,28]. Specifically, we weight the original occupation $\bar{n}_{nlms}(T)$ of each single-particle state $|nlms\rangle$ with a Lorentzian function, i.e., we modify such occupation to

$$\bar{n}_{nlms}^\gamma(T) \equiv \int_{-\infty}^{\infty} \frac{dE}{\pi} \frac{\gamma f_{\text{FD}}(E, \mu, T)}{\gamma^2 + (E - E_{nlms})^2}, \quad (8)$$

which can be integrated analytically. The magnetic susceptibility is shown in Fig. 2(b) for a sphere of $R = 3.7$ nm as a function of B_0 and of the linewidth γ normalized to the electronic energy scale for this radius, $E_0 = 2.8$ meV. The peaks in the susceptibility remain for $\gamma \lesssim 10^{-2}E_0$, where individual energy levels are well resolved. The diamagnetic response at $B_0 < B_*$ remains visible way beyond this linewidth range. The presence of a finite linewidth at $T = 0$ has, as expected, a very similar qualitative effect as a finite temperature [see Fig. 2(c) for comparison].

The quantum size effects shown in this work can be experimentally observed with ultrasensitive magnetic sensors. Here we propose two alternative experimental approaches based on $\text{YBa}_2\text{Cu}_3\text{O}_{7-\delta}$ (YBCO) nanoscopic superconducting quantum interference devices (nanoSQUIDs) [30,31], which offer a spin sensitivity of $\sim 10 \mu_B/\text{Hz}^{1/2}$ (at 1 MHz) and can operate at magnetic fields up to ~ 1 T [29,32]. In both approaches the signal from the sample is modulated at frequency $f \sim 10$ –100 kHz in order to exploit the maximum sensitivity of the nanoSQUID, and the dc magnetic field B_0 is applied parallel to the nanoSQUID loop and perpendicularly to the plane of the Josephson junctions so that no magnetic flux is coupled to them. In the first approach [inset Fig. 3(a)] the nanoparticle is attached to a cantilever and its distance to the nanoSQUID oscillates. This enables lock-in detection of the resulting modulated magnetic flux through the nanoSQUID, whose amplitude is given by $\Phi = \phi_c m_z(B_0)$ with ϕ_c the coupling factor [29]. As evidenced by Fig. 3(a), for typical values $R = 10$ nm, $T = 10$ mK, and optimum values $\phi_c = 10 \text{ n}\Phi_0/\mu_B$, with Φ_0 the magnetic flux quantum, the flux experiences steps of $\sim 3 \mu\Phi_0$. In the second approach

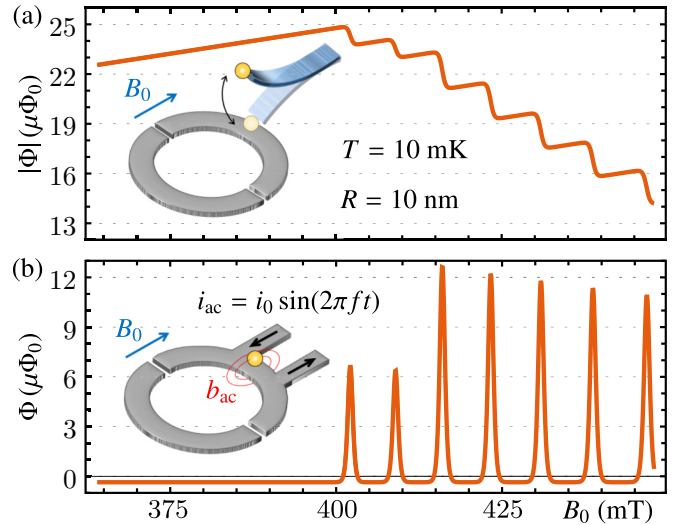


FIG. 3. Experimental proposal using a nanoSQUID. (a) The flux induced by a nanoparticle attached to an oscillating cantilever is proportional to the induced magnetic moment m_z , Eq. (4). (b) An ac current through the nanoSQUID generates an ac magnetic field at the nanoparticle position, the resulting flux being proportional to the magnetic susceptibility χ , Eq. (7). In both panels we quantitatively estimate the signal for $R = 10$ nm, $T = 10$ mK, and typical nanoSQUIDs [29].

[inset Fig. 3(b)] the particle experiences the oscillating external magnetic field $b_{\text{ac}} = b \sin(2\pi ft)$ ($b \ll B_0$) created by an ac current circulating through the nanoSQUID. The flux through the nanoSQUID contains an ac component which depends only on the excitation signal (and can be compensated electrically) plus an ac component, $\Phi_{\text{ac}}(t) = \Phi \sin(2\pi ft)$, whose amplitude $\Phi = Vb\phi_c\mu_0^{-1}\chi(B_0)$ is now proportional to the susceptibility χ [Eq. (7)]. As shown in Fig. 3(b), for the same typical parameters as above and for $b = 5.8$ mT [33], the flux shows peaks of amplitude 6–12 $\mu\Phi_0$. Both experimental approaches are feasible as the expected signal exceeds the flux noise floor of YBCO nanoSQUID sensors, $S_\Phi^{1/2} \sim 0.5 \mu\Phi_0/\text{Hz}^{1/2}$ at $f = 100$ kHz [32].

In conclusion, we have theoretically predicted strong quantum size effects on the ground-state magnetization and magnetic susceptibility of gold nanoparticles of sizes up to tenths of nanometer, which lie within the measurement capabilities of state-of-the-art magnetic sensing techniques at cryogenic temperatures. An interesting outlook of our work consists in studying the thermalization of the electron gas after a deviation from equilibrium. This could shed light into the predicted exotic internal energy equilibration in isolated nanoscopic systems [34,35].

We thank J. J. Garcia-Ripoll for his valuable suggestions. C.G.-B. acknowledges support from the European Union (PWAQUTEC, H2020-MSCA-IF-2017, Grant No. 796725). F.L. and M.J.M.-P. acknowledge funding from the Spanish MICINN Grant No. RTI2018-096075-B-C21.

- [1] W. P. Halperin, *Rev. Mod. Phys.* **58**, 533 (1986).
- [2] L. J. de Jongh, *Physics and Chemistry of Metal Cluster Compounds* (Springer, Netherlands, 1994).
- [3] F. M. Mulder, T. A. Stegink, R. C. Theil, L. J. de Jongh, and G. Schmid, *Nature (London)* **367**, 716 (1994).
- [4] R. Kubo, *J. Phys. Soc. Jpn.* **17**, 975 (1962).
- [5] L. Liz-Marzán, *Langmuir* **22**, 32 (2006).
- [6] J. M. Krans, J. M. van Ruitenbeek, V. V. Fisun, I. K. Yanson, and L. J. de Jongh, *Nature (London)* **375**, 767 (1995).
- [7] Y. Volokitin, J. Sinzig, L. J. de Jongh, G. Schmid, M. N. Vargaftik, and I. I. Moiseevi, *Nature (London)* **384**, 621 (1996).
- [8] D. B. Bivin and J. W. McClure, *Phys. Rev. B* **16**, 762 (1977).
- [9] J. M. van Ruitenbeek and D. A. van Leeuwen, *Phys. Rev. Lett.* **67**, 640 (1991).
- [10] J. M. Van Ruitenbeek and D. A. Van Leeuwen, *Mod. Phys. Lett. B* **07**, 1053 (1993).
- [11] D. A. van Leeuwen, J. M. van Ruitenbeek, G. Schmid, and L. de Jongh, *Phys. Lett. A* **170**, 325 (1992).
- [12] W. Ekardt, *Phys. Rev. B* **29**, 1558 (1984).
- [13] W. A. de Heer, *Rev. Mod. Phys.* **65**, 611 (1993).
- [14] A. L. Fetter and J. D. Walecka, *Quantum Theory of Many-Particle Systems* (Dover, New York, 2003).
- [15] T. Rangel, D. Kecik, P. E. Trevisanutto, G.-M. Rignanese, H. Van Swygenhoven, and V. Olevano, *Phys. Rev. B* **86**, 125125 (2012).
- [16] M. Gómez Vilorio, G. Weick, D. Weinmann, and R. A. Jalabert, *Phys. Rev. B* **98**, 195417 (2018).
- [17] H. Mathur and A. D. Stone, *Phys. Rev. B* **44**, 10957 (1991).
- [18] M. Faraday, *Philos. Trans. R. Soc. London* **147**, 145 (1857).
- [19] L. Scarabelli, M. Coronado-Puchau, J. J. Giner-Casares, J. Langer, and L. M. Liz-Marzán, *ACS Nano* **8**, 5833 (2014).
- [20] W. M. Wang, R. M. Stoltenberg, S. Liu, and Z. Bao, *ACS Nano* **2**, 2135 (2008).
- [21] G. Giuliani and G. Vignale, *Quantum Theory of the Electron Liquid* (Cambridge University Press, Cambridge, UK, 2005).
- [22] M. Brack, *Rev. Mod. Phys.* **65**, 677 (1993).
- [23] See Supplemental Material at <http://link.aps.org/supplemental/10.1103/PhysRevB.104.L100407> for more details on the derivation of the Hamiltonian, the perturbative expansion, the algorithm used to sort the eigenenergies, the computation of the expected magnetic dipole moment, and the impact of particle size, and which includes Refs. [14,25,36–39].
- [24] J. Perenboom, P. Wyder, and F. Meier, *Phys. Rep.* **78**, 173 (1981).
- [25] S. Y. Buhmann, *Macroscopic Quantum Electrodynamics and Ground-State Casimir, Casimir-Polder and van der Waals Forces*, Dispersion Forces (Springer, Berlin, 2012).
- [26] This holds for values of N resulting in the so-called full-shell electronic configuration [23]. The generalization to other values of N is straightforward and leads to a nonzero magnetization at zero field.
- [27] F. von Oppen, *Phys. Rev. B* **50**, 17151 (1994).
- [28] H.-P. Breuer and F. Petruccione, *The Theory of Open Quantum Systems* (Clarendon, Oxford, 2010).
- [29] M. J. Martínez-Pérez, B. Müller, D. Schwebius, D. Korinski, R. Kleiner, J. Sesé, and D. Koelle, *Supercond. Sci. Technol.* **30**, 024003 (2016).
- [30] M. J. Martínez-Pérez and D. Koelle, *Phys. Sci. Rev. B*, 20175001 (2017).
- [31] C. Granata and A. Vettoliere, *Phys. Rep.* **614**, 1 (2016).
- [32] T. Schwarz, R. Wölbing, C. F. Reiche, B. Müller, M. J. Martínez-Pérez, T. Mühl, B. Büchner, R. Kleiner, and D. Koelle, *Phys. Rev. Appl.* **3**, 044011 (2015).
- [33] According to our simulations, this is the field generated at a height 100 nm above a 200-nm-wide \times 80-nm-thick nanoSQUID [29] by an ac current of amplitude $i_0 = 5$ mA.
- [34] A. E. Rubio López, C. Gonzalez-Ballester, and O. Romero-Isart, *Phys. Rev. B* **98**, 155405 (2018).
- [35] J. R. M. Saavedra, A. Asenjo-García, and F. J. García de Abajo, *ACS Photonics* **3**, 1637 (2016).
- [36] J. J. Sakurai and J. Napolitano, *Modern Quantum Mechanics* (Pearson, Harlow, 2014).
- [37] *Handbook of Mathematical Functions: With Formulas, Graphs, and Mathematical Tables*, edited by M. Abramowitz and I. A. Stegun (Dover, New York, 1972).
- [38] T. G. Pedersen, *Phys. Rev. A* **99**, 063410 (2019).
- [39] J. K. Bloomfield, S. H. P. Face, and Z. Moss, [arXiv:1703.06428](https://arxiv.org/abs/1703.06428).